Downloaded from rsif.royalsocietypublishing.org on August 20, 2010

JOURNAL OF THE ROYAL SOCIETY Interface

Deformation micromechanisms of collagen fibrils under uniaxial tension

Yuye Tang, Roberto Ballarini, Markus J. Buehler and Steven J. Eppell

J. R. Soc. Interface 2010 **7**, 839-850 first published online 6 November 2009
doi: 10.1098/rsif.2009.0390

References **This article cites 60 articles, 6 of which can be accessed free**
http://rsif.royalsocietypublishing.org/content/7/46/839.full.html#ref-list-1

Rapid response Respond to this article
http://rsif.royalsocietypublishing.org/letters/submit/royinterface;7/46/839

Subject collections Articles on similar topics can be found in the following collections

biomaterials (143 articles)
biomechanics (129 articles)
biomedical engineering (185 articles)

Email alerting service Receive free email alerts when new articles cite this article - sign up in the box at the top right-hand corner of the article or click **here**

To subscribe to *J. R. Soc. Interface* go to: **http://rsif.royalsocietypublishing.org/subscriptions**

This journal is © 2010 The Royal Society

Downloaded from rsif.royalsocietypublishing.org on August 20, 2010

JOURNAL OF THE ROYAL SOCIETY Interface

J. R. Soc. Interface (2010) **7**, 839–850
doi:10.1098/rsif.2009.0390
Published online 6 November 2009

Deformation micromechanisms of collagen fibrils under uniaxial tension

Yuye Tang[1], Roberto Ballarini[1,*], Markus J. Buehler[2,*] and Steven J. Eppell[3,*]

[1]*Department of Civil Engineering, University of Minnesota, Minneapolis, MN 55455, USA*
[2]*Laboratory for Atomistic and Molecular Mechanics, Department of Civil and Environmental Engineering, Massachusetts Institute of Technology, Cambridge, MA 02139, USA*
[3]*Department of Biomedical Engineering, Case Western Reserve University, Cleveland, OH 44106, USA*

Collagen, an essential building block of connective tissues, possesses useful mechanical properties due to its hierarchical structure. However, little is known about the mechanical properties of collagen fibril, an intermediate structure between the collagen molecule and connective tissue. Here, we report the results of systematic molecular dynamics simulations to probe the mechanical response of initially unflawed finite size collagen fibrils subjected to uniaxial tension. The observed deformation mechanisms, associated with rupture and sliding of tropocollagen molecules, are strongly influenced by fibril length, width and cross-linking density. Fibrils containing more than approximately 10 molecules along their length and across their width behave as representative volume elements and exhibit brittle fracture. Shorter fibrils experience a more graceful ductile-like failure. An analytical model is constructed and the results of the molecular modelling are used to find curve-fitted expressions for yield stress, yield strain and fracture strain as functions of fibril structural parameters. Our results for the first time elucidate the size dependence of mechanical failure properties of collagen fibrils. The associated molecular deformation mechanisms allow the full power of traditional material and structural engineering theory to be applied to our understanding of the normal and pathological mechanical behaviours of collagenous tissues under load.

Keywords: collagen mechanics; collagen fibril; mesoscopic model; failure micromechanism; size effect

1. INTRODUCTION

Fibril-forming collagens, the most abundant proteins in mammals, are found in tissues such as skin, tendon and bone. The superstructures into which these molecules self-assemble possess useful mechanical properties including high tensile strength around 1 GPa and great extensibility reaching up to 100 per cent strain before fracture (Shen *et al.* 2008). Exploring how molecular-level interactions conspire to produce tissue-level mechanical response of collagenous materials provides a promising avenue for advancing medical diagnosis/treatment and tissue engineering.

The structure of collagen extends over several length scales, as sketched in figure 1. The fundamental elements of collagen are amino acid sequences arranged in the pattern (–Gly–X–Y–), where in approximately 20 per cent of all cases, X and Y are Pro and Hyp, respectively (Parry 1988; Kadler *et al.* 1996). The amino acid sequences constitute a left-handed polypeptide helix, three of which assemble in parallel into a right-handed supercoil producing the tropocollagen (TC) molecule. A TC molecule is approximately 300 nm long, 1–2 nm in diameter and weighs 300 kDa (Rice *et al.* 1964; Parry 1988; Kadler *et al.* 1996; Ottani *et al.* 2002; Buehler 2006*b*). The detailed molecular topography of short peptide fragments that model certain aspects of the naturally occurring fibrillar collagen molecules has been determined from X-ray diffraction experiments (Bella *et al.* 1994; Kramer *et al.* 2000). The molecular structure of such a model peptide is shown in figure 1 as an example (protein data bank code 1QSU; Kramer *et al.* 2000). TC molecules aggregate into fibrils and are stabilized via intermolecular adhesion and covalent cross-links at their ends (through lysine, allysine, hydroxylysine and hydroxyallysine residues; Lodish *et al.* 1999; Bailey 2001; Alberts *et al.* 2002). The two-dimensional collagen fibril considered in this study follows the Hodge–Petruska arrangement (Hodge & Petruska 1963) depicted in figure 1. TC molecules are grouped into a staggered structure with an axial offset distance $D = 67$ nm and an equilibrium centre-to-centre distance of 1.5 nm between nearest neighbour molecules. The total length of a TC molecule is approximately $4.34D$, and the gap between amino and carboxy termini of two molecules in the same row is approximately $0.6D$. This D period was determined through transmission electron microscopy (Schmitt

*Authors for correspondence (broberto@umn.edu; mbuehler@mit.edu; sje@case.edu).

Received 2 September 2009
Accepted 13 October 2009

This journal is © 2009 The Royal Society

Downloaded from rsif.royalsocietypublishing.org on August 20, 2010

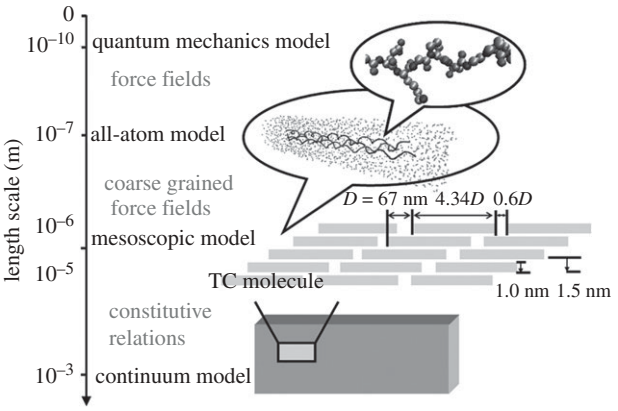

Figure 1. Schematic view of the hierarchical structure of collagen, from nano to macro. The present study is focused on collagen fibrils at scales of 10^{-6}–10^{-5} m.

et al. 1942). Important extensions of the Hodge–Petruska scheme to a three-dimensional generalized packing model were achieved in the mid-1980s (Lees *et al.* 1984*a*,*b*; Bonar *et al.* 1985; Lees 1986, 1987) based on pioneering neutron diffraction studies on mineralized and non-mineralized collagenous tissue. More recent efforts include the work of Gutsmann *et al.* (2003) and Bozec *et al.* (2007). While recent experimental evidence (Orgel *et al.* 2006) revealed a three-dimensional twisted right-handed crystallographic structure of collagen microfibrils, we have not included this in the model presented below. Finally, collagen fibrils assemble into distinct types of biological tissues through larger scale structural assemblies.

The mechanical properties of hierarchical collagenous structures ranging from individual collagen molecules to large-scale macroscopic connective tissues have received significant attention: theoretical (Soulhat *et al.* 1999; Jager & Fratzl 2000; Hellmich *et al.* 2004; Wilson *et al.* 2004, 2005; Freed & Doehring 2005; Fritsch & Hellmich 2007; Nikolov & Raabe 2008; Fritsch *et al.* 2009; Tang *et al.* 2009), experimental (Abrahams 1967; Diamant *et al.* 1972; Akizuki *et al.* 1986; Folkhard *et al.* 1987; Bigliani *et al.* 1992; Misof *et al.* 1997; Fratzl *et al.* 1998; Purslow *et al.* 1998; Catanese *et al.* 1999; Christiansen *et al.* 2000; Sun *et al.* 2002, 2004; Gentleman *et al.* 2003; Gutsmann *et al.* 2004; Bozec & Horton 2005; Wenger *et al.* 2007; Shen *et al.* 2008) and computational (Li *et al.* 2000; Mooney *et al.* 2001, 2002; Wilson *et al.* 2004, 2005; Israelowitz *et al.* 2005; Lorenzo & Caffarena 2005; Buehler 2006*a*,*b*; Buehler & Wong 2007; Buehler 2008; Veld & Stevens 2008).

Challenges in computational mechanics modelling of collagenous assemblies lie in the numerous distinct length scales involved in their structural makeup and in the intimate coupling between chemistry, biology and mechanical deformation. Fully atomistic simulation of macroscopic collagenous tissues is currently impossible, and therefore multi-scale analysis has been developed into a promising tool that relies on a hierarchically coupled treatment of each of the scales. For example, molecular dynamics (MD) simulations of stretching, bending and shearing of TC molecules and small fibrillar assemblies thereof (Buehler 2006*a*; Buehler & Wong 2007) relied on potentials constructed from the results of quantum chemistry calculations and reactive force fields. This bottom-up approach was used to investigate entropic effects on the mechanical behaviours of long contorted TC molecules (Buehler 2006*a*; Buehler & Wong 2007) as well as collagen fibrils assembled using the Hodge–Petruska scheme (Buehler 2006*b*, 2008).

What has not yet been explored in a systematic fashion using MD modelling is the complex interaction among collagen fibril length, width and cross-linking density. For example, earlier simulations based on a two-dimensional mesoscopic model showed that the uniaxial stress–strain responses of collagen fibrils containing two molecules along their length and with periodicity in the width direction are greatly affected by the cross-linking density (Buehler 2008). Highly cross-linked fibrils demonstrated higher yield strength and brittle failure. Fibrils with low cross-linking exhibited a graceful failure involving a strain softening (decreasing stress with increasing strain) post-peak region. The study did not, however, consider whether the computational experiment was performed on a representative volume element (RVE). (The model behaves as an RVE if the mechanical behaviour is independent of the size of a sample.) Here, we use the same two-dimensional mesoscopic model to study the effects of fibril dimensions and cross-linking density on mechanical response, with particular attention on whether a collagen fibril of a given size can be considered an RVE (and at what scale), and whether graceful failure can be achieved in fibrils containing more than a few molecules along their length or width. The computed responses are used to construct a continuum strength model and curve-fitted equations for fibril yield stress, yield strain and fracture strain.

2. MESOSCOPIC SIMULATIONS

2.1. Model and methods

To overcome the limitations imposed by the enormous number of degrees of freedom that would be required for an all-atom simulation of a collagen fibril, the mesoscopic model (figure 2*a*) serves as the primary simulation tool used here (Buehler 2006*a*,*b*, 2008). The coarse-grained model describes TC molecules as chains of interacting beads (i.e. point masses) that represent the atomistic structure, which enables a sufficiently accurate treatment of long-range responses of collagen fibrils under mechanical stress. The intramolecular properties of individual TC molecules (i.e. the bond potential and angle potential among beads) and the interaction between TC molecules (i.e. the non-bonded potential among beads) are determined from the results of atomistic simulation using reactive force fields with a pure water phase (Buehler 2006*a*). Intermolecular cross-links are formed in the highlighted regions shown in figure 2*a*. Cross-linking is incorporated in the model by locally enhancing the adhesion forces between molecules β-fold, with $\beta = 1$ corresponding to

Downloaded from rsif.royalsocietypublishing.org on August 20, 2010

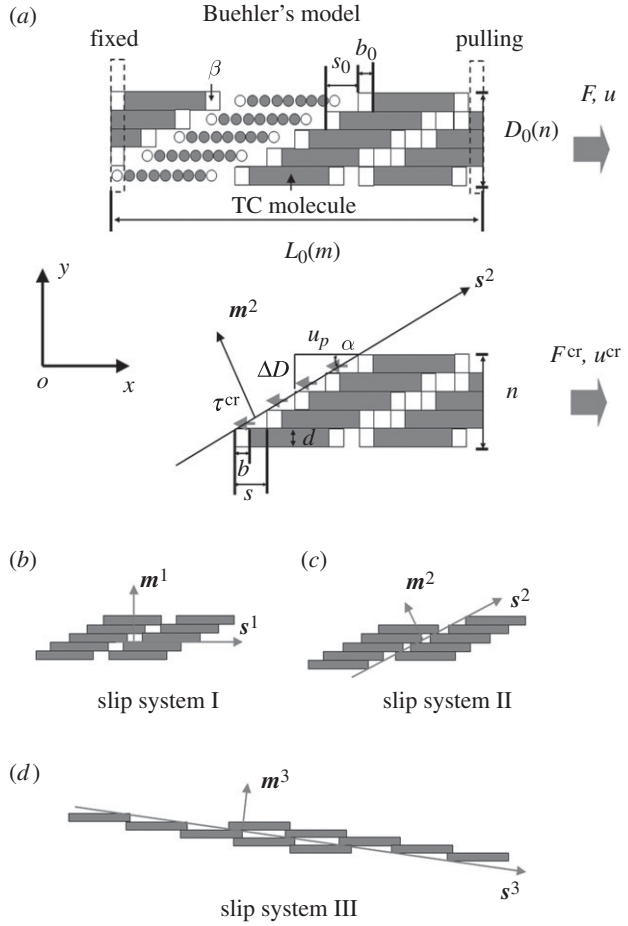

Figure 2. (*a*) Schematic plot of the two-dimensional staggered collagen model. The parameters m and n are variables, which lead to different lengths and widths of the specimen. (*b–d*) Definition of possible slip systems in the collagen structure. $\boldsymbol{m}^{(\alpha)}$ and $\boldsymbol{s}^{(\alpha)}$ represent the normal of slip plane and slip direction.

no cross-linking. Varying β enables us to model different cross-link densities. The coarse-grained simulations were carried out using the MD simulator LAMMPS (Plimpton 1995).

We note that a molecular-level model of the cross-link structure (with atomistic resolution) is being developed, based on experimental data on the chemistry and location of cross-links in the fibril arrangement. Once developed, this model will enable us to probe the effects of cross-links on the mechanical behaviour of collagen fibrils from a more fundamental perspective than what is done in this paper.

A detailed description of the two-dimensional mesoscopic model of collagen fibrils is included in earlier publications (Buehler 2006*a*; Buehler & Wong 2007). Regarding the effect of water (and other solvents), the full atomistic simulations that are used to extract parameters for the coarse-grained model are carried out in explicit water solvent (see earlier papers by Buehler *et al.*). As such, they directly include the effect of water solvent. For any larger scale effects of water (e.g. nano/microfluidic mechanisms that occur at the fibril scale), the mesoscale model could in principle be reformulated to include explicit water as well; however, this is beyond the scope of current studies. Initial attempts by the authors have been made by using the coarse-grained MARTINI force field, based on which we are currently building a microscale model of a fibril with explicit water.

As shown in figure 2*a*, the dimensions of the fibril are defined by the number of TC molecules along the length, $m = 2–10$, and across the width, $n = 2–20$. In subsequent discussion, the fibril size is thus defined as $m \times n$, and β is varied from 1 to 50. The nominal strain ε_x, defined as the extension, u, divided by the initial length of the fibril, L_0, and nominal stress, σ_x, determined by dividing the virial stress by the initial volume of the collagen fibril (i.e. $D_0 L_0 d$, where D_0 and d are the initial width and thickness of the specimen), are tracked throughout the simulation.

Visualization of the molecular deformation mechanisms within the fibril is facilitated by using the slip vector approach (Zimmerman *et al.* 2001), with the slip vector $\boldsymbol{\delta}^i$ defined as

$$\boldsymbol{\delta}^i = -\frac{1}{\zeta_s}\sum_{j\neq i}^{\zeta}(\mathbf{x}^{(ij)} - \mathbf{X}^{(ij)}), \tag{2.1}$$

where $\mathbf{x}^{(ij)}$ and $\mathbf{X}^{(ij)}$ are the vector differences between the coordinates of beads i and j in the current and reference states, respectively, ζ is the number of nearest neighbours (the beads spatially closest) to bead i in the reference state and ζ_s is the number of slipped neighbours (neighbour beads that slip along a slip plane adjacent) to bead i in the current state. The reference state is taken as the zero mechanical stress configuration at the beginning of the simulation.

2.2. Results

2.2.1. Short fibrils with varying cross-linking density. The first example involves a 2×5 fibril. The same structure, but with periodic boundary conditions across its width, was considered in a previous study focused on the effects of varying cross-linking density (Buehler 2008). Here, we consider a finite geometry by removing the periodicity constraints and present the results in figure 3.

The stress–strain curves for cross-linking in the range $1 \leq \beta < 20$ are linear elastic and exhibit a small strain modulus of approximately 5 GPa. For higher levels of cross-linking, $\beta \geq 20$, the curves are approximately bilinear with an elastic modulus of approximately 35 GPa activated at a strain of approximately 0.32. After yielding at strains in the range of 0.06–0.42, except for $\beta = 40$ the fibrils display a graceful failure as evidenced by either post-peak yielding at constant stress or strain softening. The most highly cross-linked fibril fails in a brittle fashion at a failure strain, ε^f, approximately equal to 0.42, whereas the graceful failures are associated with $\varepsilon^f = 0.64–1.03$. These results are consistent with those of the periodic structure (Buehler 2008).

The stress–strain curves result from the competition between fracture of TC molecules and fracture of cross-links as well as sliding of TC molecules thereafter (Buehler 2006*b*, 2008). For high-density cross-links, TC molecules rupture at a critical force, leading to the brittle failure of the collagen fibril. The breaking

Downloaded from rsif.royalsocietypublishing.org on August 20, 2010

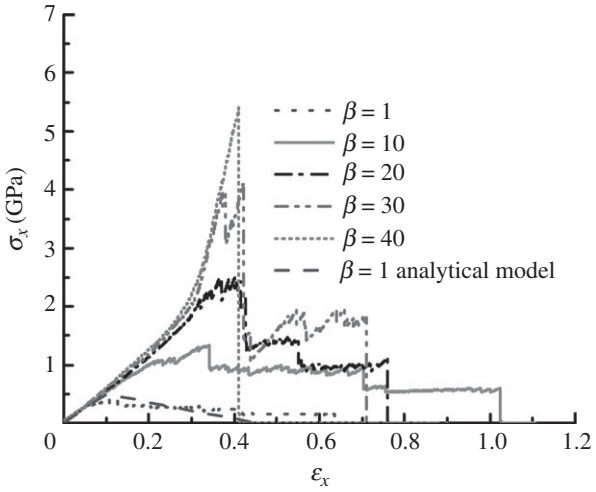

Figure 3. Stress–strain curves of the 2×5 collagen fibril with various cross-linking densities.

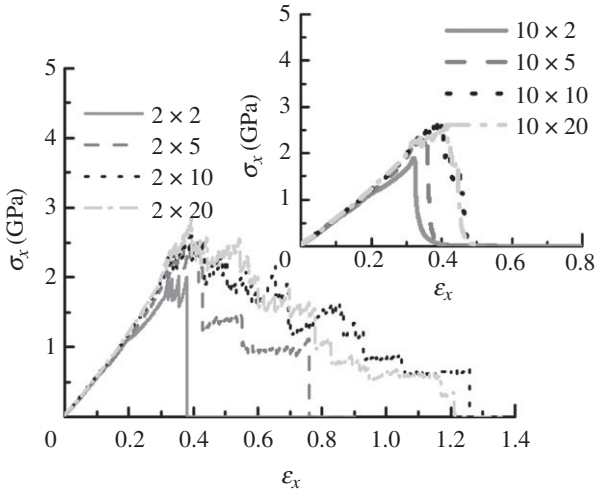

Figure 4. Stress–strain curves of $2 \times n$ collagen fibrils with cross-linking density $\beta = 20$. The parameter n changes from 2 to 20.

of low-density cross-links, on the other hand, leads to sliding of TC molecules and strain softening.

These results alone suggest that high (low) levels of cross-linking make collagen fibrils brittle (ductile). As we will see in the next section, this is not true when fibrils of different sizes are considered.

2.2.2. Effects of length and width. We next study the effects of fibril length and width for an intermediate value of $\beta = 20$, focusing on whether the fibrils approach an RVE and whether they are brittle or ductile. Figure 4 shows that the previously calculated short fibril ($m = 2$) becomes an RVE (where the stress–strain curve is independent of width) for $n > 10$. The deviation of the stress–strain curve of the 2×2 fibril at a strain of 0.19 is a result of strong boundary effects. Increasing n from 2 to 20 eliminates the effects of the boundary and leads to a subtle increase in the tangent elastic modulus, yield strength and yield strain, and a more pronounced increase in dissipated energy. We note that the fracture strain approaches approximately 1.2 for large n. The inset in figure 4, corresponding to $m = 10$, shows again that RVE behaviour is achieved for $n > 10$. Notably, this plot also shows that graceful failure cannot be achieved by fibrils of this length, regardless of the influence of cross-linking density discussed in §2.2.1. These results suggest that collagen fibrils, which typically contain large numbers of molecules along their lengths, are expected to fail in a brittle manner (results for other values of β are presented in §3.2). As will be discussed in §2.4, this transition from stable to unstable structural behaviour is analogous to that of a fibre-shaped continuum that contains (or develops) a propagating crack.

Figure 5 shows the results for $n = 5$ and varying m. Because the 5×5 and 10×5 collagen fibrils essentially resemble an in-series arrangement of the 2×5 configuration, the tangential moduli in these plots are similar. They yield at a strain of approximately 0.32 and at a stress of approximately 2 GPa. The transition from graceful to brittle failure is clearly seen for increasing fibril length.

2.3. Deformation mechanisms

Consider first the deformation history of fibrils that exhibit a graceful failure, such as the 2×5, $\beta = 20$ fibril shown in figure 5. The fibril's response is divided into two stages: stage I corresponds to a smooth linear elastic response up to yield and stage II to a step ladder-shaped strain softening post-peak region. Reference points in the pre-peak and post-peak regions are labelled a–f, and the corresponding snapshots of the mesoscopic collagen configurations for these points are shown in figure 6*a–f*.

The undeformed structure is shown in figure 6*a*. A full atomistic simulation of tropocollagen molecules shows that the deformation from a to b can be fully explained by molecular stretching and uncoiling of the triple helical protein structures (Buehler & Wong 2007). The configuration corresponding to point b indicates an increase in distance between material points ① and ⑦ thus an extension of TC molecules. Concomitantly, intermolecular interactions result in the bending of TC molecules at the gap regions. Further loading from point b to point c leads to stretching of the covalent bonds in the collagen structure and is met by a slight increase in stiffness (Buehler 2006*b*, 2008). At point c, the collagen structure begins to yield, and the structural configuration at this critical moment is depicted in figure 6*c*.

The failure of the collagen fibril is caused by rupturing of TC molecules or breaking of cross-links, and relative slip between TC molecules. In this specific example, the loads do not exceed the elastic limit of any single TC molecule. Instead, cross-links reach their maximum fracture stress, and slip motions take place at the most vulnerable positions of the collagen structure, resulting in the whole fibril experiencing unloading (the drops in the post-peak region in figure 5). Although the fibril did not contain pre-existing defects, dislocation-type slip of TC molecules occurs due to the staggered nature of the fibril (figure 2*a*), using a previously described mechanism (Buehler 2006*b*). Three slip systems, I, II and III, are

Downloaded from rsif.royalsocietypublishing.org on August 20, 2010

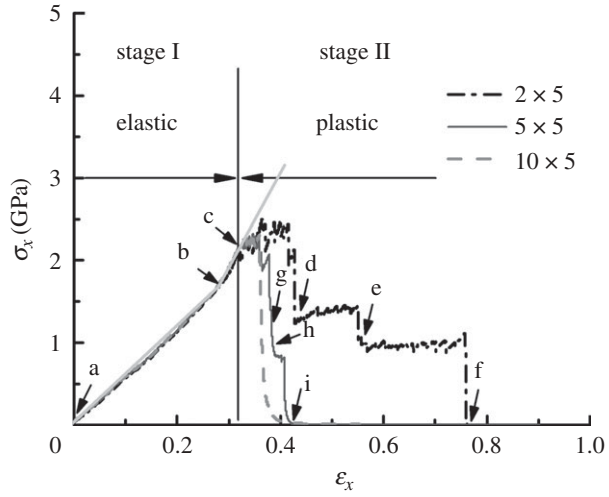

Figure 5. Stress–strain curves of $m \times 5$ collagen fibrils with cross-linking density $\beta = 20$. The parameter m changes from 2 to 10. Different snapshots along the deformation histories of the 2×5 and 5×5 collagen fibrils are labelled from a to i and corresponding visualizations are shown in figures 6 and 9.

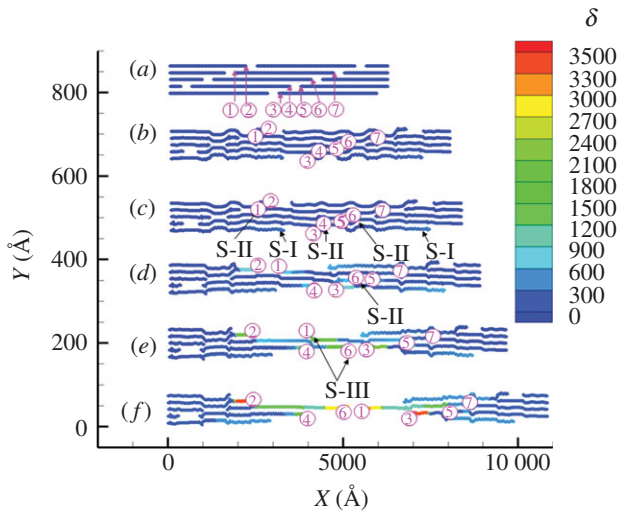

Figure 6. (*a–f*) Snapshots of the 2×5 fibril configurations at points a to f in figure 5. ①–⑦ define material points in the collagen structure marked to visualize elastic extension and the slip motions of TC molecules. S-I, S-II and S-III stand for the types I–III slips shown in figure 2*b–d*. (*d–f*) Snapshots capture the final configurations of the fibril after slips initiated (labelled) in (*c–e*).

described by the arrangement of molecules shown in figure 2*b–d*, where $\boldsymbol{m}^{(\alpha)}$ and $\boldsymbol{s}^{(\alpha)}$ represent the normal to the slip plane and the slip direction, respectively. Development of these slip systems provides a molecular scale mechanism that describes the post-peak softening behaviour of the fibril.

To quantify the slip motions in the collagen fibril, the magnitude of the slip vectors is computed for each bead in the structure and the resulting contours superimposed on the fibril in figure 6. By tracking the trajectories of selected beads, we observe type I slips along the fibril surface all through the post-peak deformation. However, only the relative movements of beads ①–⑥ lead to softening. The collagen fibril initiates type II slips in figure 6*c*. Points ①, ③ and ⑤ switch their orders with ②, ④ and ⑥, respectively. This results in a steep reduction in stress at point d and the localized deformation shown in figure 6*d*. Subsequently, type II slip occurs again only at positions ③ and ⑥, leading to a further stress drop at point e. In figure 6*e*, two TC molecules remain where the deformation localizes. Finally, type III slip occurs at the new positions ① and ⑥, resulting in fracture at point f.

2.4. *Plausible explanation of the brittle-to-ductile transition*

The results in §2.2.2 clearly illustrate that fibril length and width determine whether the structural response after the peak stress is stable (i.e. the stress–strain curve is associated with a gradual decrease in stress with increasing strain) or unstable (i.e. the stress–strain curve terminates at the peak stress). One way of thinking about the transition from stable to unstable response involves an analogy between the hierarchical fibril and a continuum beam containing a crack (figure 7) whose equilibrium length is dictated by the Griffith condition (the applied energy release rate, defined as the change with respect to crack length of the work of the applied force minus the strain energy, is equal to the critical energy release rate that is required to propagate the crack). Consider the normalized stress–displacement response of a tension-loaded edge-cracked beam. The edge crack in this continuum represents the numerous crack-like regions that develop as bonds break and molecules slide, and the cross-sectional area is reduced in the MD simulation of the fibril. The response before the initial crack starts to propagate is linear up to the stress that renders the applied energy release rate equal to the critical energy release rate. For relatively small aspect ratios ($L_0/D_0 = 0.2$–1.0), Griffith equilibrium is maintained by a decreasing stress and a concomitant increase in displacement. For relatively large aspect ratios ($L_0/D_0 = 2$–4), however, a balance between the applied energy release rate and the critical energy release rate requires a negative increment in the work of the applied load. This results in a post-peak response involving snap-back instability. The snap-back cannot be captured in a displacement-controlled experiment or simulation such as the ones performed in this study; for those specimens that may be associated with such unstable structural response, displacement control forces the post-peak response to jump vertically to the equilibrium path (which approaches zero stress for increasing aspect ratios).

Furthermore, the transition can also be understood by considering the deformation mechanisms. The MD simulations suggest that failure of a collagen fibril is localized within several specific slip planes. During the softening stage, if the elastic strain decreases faster than the accumulation of plastic strain in the localization region(s), snap-back is found in the stress–strain curve (Jirasek & Bazant 2001). Otherwise, the fibril experiences a graceful failure. Figure 8 depicts the configurations at the onset of fracture of collagen fibrils whose stress–strain curves were depicted in figure 4. For the 2×2 fibril, brittle fracture is caused by a type II slip between two contacting TC molecules.

Downloaded from rsif.royalsocietypublishing.org on August 20, 2010

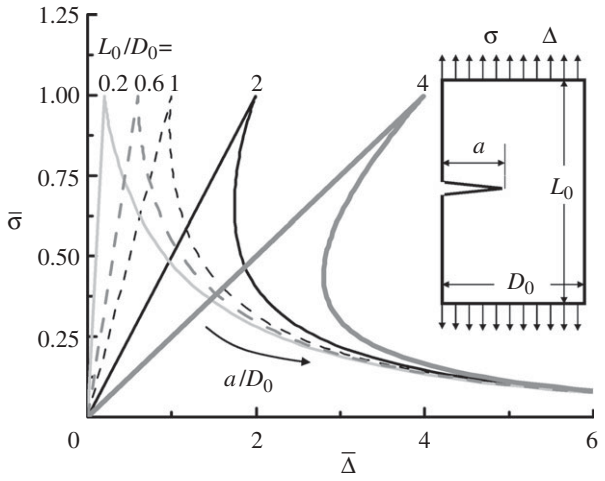

Figure 7. Illustration of the brittle-to-ductile transition of a plate containing an edge crack. Changing L_0/D_0 results in different normalized stress–strain curves.

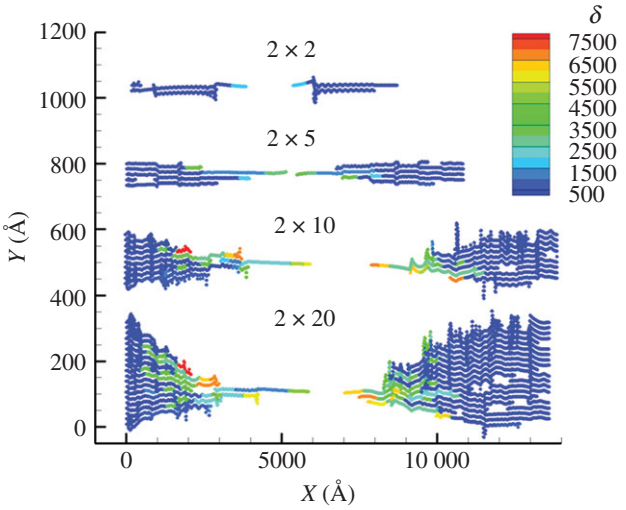

Figure 8. Snapshots of the configurations of the 2 × 2, 2 × 5, 2 × 10 and 2 × 20 collagen fibrils ($\beta = 20$) at fracture points in figure 4.

The softening response of the 2 × 5 fibril, decomposed and illustrated in §2.3, involves multiple slips of types I–III. For fibrils with larger width (2 × 10 and 2 × 20), more slip motions are observed at different positions in figure 8. The increasing number and magnitude of slips indicate that more plastic strain accumulates while unloading. Hence, fibrils with larger widths dissipate more energy as a result of a graceful post-peak region terminating at larger fracture strains. Figure 9 presents snapshots of the 5 × 5 collagen fibril corresponding to the points marked in figure 5. The sequence and magnitudes of the slip motions of this fibril are similar to those of the 2 × 5 fibril. This implies that a smaller amount of plastic strain accumulates in the 5 × 5 fibril, resulting in more brittle behaviour. Because our simulations are displacement controlled, the snap-back instability that may be associated with a relatively long fibril ($m \geq 10$ in this example) is not captured, and the fibril fails catastrophically at the onset of yielding.

It is clear that the variation of the stress–strain curve with fibril size is structurally describable using relative slip between the collagen molecules. These observations provide the basis for the simple analytical model presented next.

3. MODELS

3.1. Analytical model

A model for the yield stress and fracture strain capable of transitioning from brittle to graceful failure can be constructed according to the $m \times n$ staggered collagen fibril structure shown in figure 2*a*. The left end of the fibril is fixed and its right end is loaded by a force F. The molecules are assumed to be linear elastic. For the rising portion of the stress–strain we assume that the total extension u equals the elastic extension u_e. The force is thus

$$F = \bar{E}u_e\frac{A_0}{L_0} = \bar{E}u\frac{A_0}{L_0}, \tag{3.1}$$

where A_0 and L_0 are, respectively, the initial cross-sectional area and the initial length of the staggered fibril structure. For the plane stress model considered here, A_0 equals $D_0 d$. The equilibrium distance between rows of TC molecules, d (shown in figure 2*a*), can be regarded as the thickness of the fibril, $D_0 = nd$ is the initial width of the structure and $\bar{E}$ is the effective elastic modulus of the cross-linked TC molecules.

In the range $1 < \beta < 40$, cross-links break at a critical force F^{cr}. Consider the simplest case involving only type II slip (figure 2*a*). At the onset of yielding, $n-1$ pairs of TC molecules are in contact. F^{cr} is related to the maximum intermolecular adhesion line force τ^{cr} through

$$F^{cr} = (n-1)\tau^{cr}b_0 = \left(\frac{D_0}{d} - 1\right)\tau^{cr}b_0, \tag{3.2}$$

where b_0 is the initial contact length between two TC molecules at ends illustrated in figure 2*a*. We define the normalized width $\hat{D} = n = D_0/d$ and the normalized maximum adhesion force $\hat{\tau} = \tau^{cr}b_0/(\bar{E}d^2)$. The corresponding critical nominal stress $\bar{\sigma}_x^{cr}$ (i.e. yield strength) becomes

$$\bar{\sigma}_x^{cr} = \frac{F^{cr}}{A_0} = \bar{E}\hat{\tau}\left(1 - \frac{1}{\hat{D}}\right). \tag{3.3}$$

The total force applied after yielding can be written as

$$F = \left(\frac{d}{D} - 1\right)\tau^{cr}b_0 = \left(\frac{D_0 - \Delta D}{d} - 1\right)\tau^{cr}b_0, \tag{3.4}$$

where D and ΔD are, respectively, the diameter and its change at the section experiencing localization. Defining α as the angle of the slip plane in the deformed coordinates for large deformation, $\Delta D = u_p \tan\alpha$ (figure 2*a*). The plastic deformation after yielding, u_p, equals the total extension minus the elastic deformation of the fibril, $u_p = u - u_e = u - FL_0/(A_0\bar{E})$. Substituting these last two relations into equation (3.4), the relationship between external force and total extension after yielding becomes

$$F = \frac{(D_0 - d) - u\tan\alpha}{d/(b_0\tau_{cr}) - L_0\tan\alpha/(D_0 d\bar{E})}. \tag{3.5}$$

Downloaded from rsif.royalsocietypublishing.org on August 20, 2010

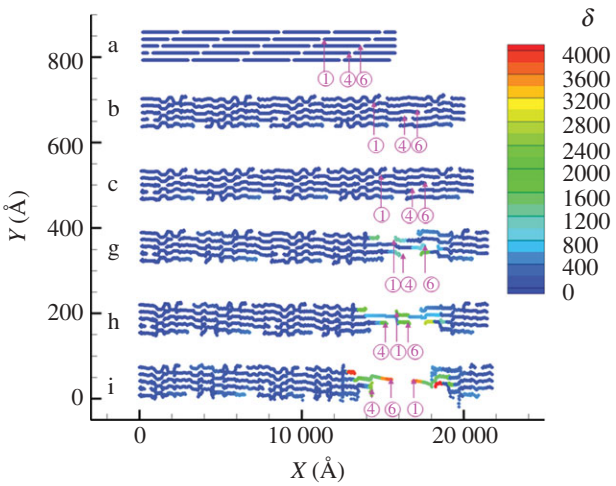

Figure 9. Snapshots of the 5×5 fibril configurations ($\beta = 20$) at points a to c and g to i in figure 5. ①, ④ and ⑥ are material points in the collagen structure marked to visualize elastic extension and the slip motions of TC molecules.

We note that $\tan\alpha = d/s$, where s, the deformed length shown in figure 2*a*, is estimated from its initial length s_0:

$$s = s_0(1+\varepsilon^{\mathrm{cr}}) = s_0\left(1+\frac{\bar{\sigma}_x^{\mathrm{cr}}}{\bar{E}}\right) = s_0\left[1+\hat{\tau}\left(1-\frac{1}{\hat{D}}\right)\right]. \tag{3.6}$$

By defining the normalized length, $\hat{L} = L_0/s_0$, equations (3.1) and (3.5) can be represented in terms of nominal stress and strain as

$$\bar{\sigma}_x = \begin{cases} \bar{E}\varepsilon_x & \text{(elastic)} \\ \dfrac{\bar{E}(\varepsilon^{\mathrm{f}}-\varepsilon_x)}{[\hat{D}(1+1/\hat{\tau})-1]/\hat{L}-1} & \text{(plastic).} \end{cases} \tag{3.7}$$

The associated fracture strain is

$$\varepsilon^{\mathrm{f}} = \frac{D_0-d}{L_0\tan\alpha} = \frac{(n-1)s}{L_0} = \frac{(\hat{D}-1)+\hat{\tau}(\hat{D}+1/\hat{D}-2)}{\hat{L}}. \tag{3.8}$$

The model captures the transition from brittle to graceful failure, as evidenced by the inverse-length dependence of the fracture strain. Qualitatively, $\bar{\sigma}_x^{\mathrm{cr}}$ increases with increasing $\hat{\tau}$ and $\hat{D}$, and ε^{f} decreases with decreasing $\hat{D}$ and $\hat{\tau}$ or increasing $\hat{L}$. The predictions can be assessed by using the parameters developed previously through MD simulation of a 2×5 collagen fibril with $\beta = 1$: $\tau^{\mathrm{cr}} \approx 5.55$ pN Å^{-1}, $\bar{E} = 5$ GPa, $L_0 = 6200$ Å, $d = 16.3$ Å, $b_0 = 300$ Å and $s_0 = 630$ Å (Buehler 2006*a*; Buehler & Wong 2007). The bilinear stress–strain curve predicted by the model, plotted in figure 3, is defined by $\bar{\sigma}_x^{\mathrm{cr}} = 0.5$ GPa and $\varepsilon^{\mathrm{f}} = 0.45$. The peak stress is reasonably captured, while the fracture strain is underestimated because the model does not include the multiple slips of types I–III observed in the MD simulation.

Table 1. Coefficients of the phenomenological model.

equation (3.9)		equation (3.10)		equation (3.11)	
p_1	0.020983	q_1	0.45698	t_1	0.840038
p_2	−0.03169	q_2	−0.4101	t_2	0.979366
p_3	0.009651	q_3	19.72913	t_3	0.005424
p_4	0.03737			t_4	0.295104
p_5	−0.01041			t_5	2.771249
p_6	0.001012			t_6	0.093824
p_7	−0.50187			t_7	0.161244
p_8	0.065954			t_8	−6.22646
p_9	0.043451			t_9	0.336629
p_{10}	−0.01435			t_{10}	2.629326
p_{11}	0.001621			t_{11}	3.349119
				t_{12}	−0.10898
				t_{13}	0.012663
				t_{14}	197.5329
				t_{15}	−40.9788

3.2. Phenomenological model

Extensive numerical analyses were performed involving $\beta = 1$–50, $m = 2$–10 and $n = 2$–20 in order to train the phenomenological model based on the molecular simulation results. The average run time of one serial simulation on the IBM Blade Cluster at the University of Minnesota Supercomputer Institute is approximately 50 h. Performing parameter studies on larger values of m and n will be one of our future directions. Data-fitting equations for the normalized yield strength $\sigma^{\mathrm{y}}/E_{\mathrm{TC}}$, yield strain ε^{y} and fracture stress ε^{f} are presented and discussed next. These expressions reflect the overall trends of the characteristic properties and can be useful to those researchers who do not have the resources to perform MD simulations. $E_{\mathrm{TC}} \sim 6.2$ GPa is the elastic modulus of a single TC molecule under small deformation in the uniaxial tension test (Buehler & Wong 2007). The results suggest that $\sigma^{\mathrm{y}}/E_{\mathrm{TC}}$ is a strong function of β, a weak function of n and insensitive to m and can be written as

$$\frac{\sigma^{\mathrm{y}}}{E_{\mathrm{TC}}} = \frac{p_1+p_2\ln\beta+p_3(\ln\beta)^2+p_4\ln n+p_5(\ln n)^2+p_6(\ln n)^3}{1+p_7\ln\beta+p_8(\ln\beta)^2+p_9\ln n+p_{10}(\ln n)^2+p_{11}(\ln n)^3}. \tag{3.9}$$

Yield strain ε^{y} depends on β according to

$$\varepsilon^{\mathrm{y}} = q_1 + q_2\exp\left(\frac{-\beta}{q_3}\right). \tag{3.10}$$

The coefficients that enter equations (3.9) and (3.10) are listed in table 1.

The results of the simulations and their associated fitting curves are shown in figure 10. While $\sigma^{\mathrm{y}}/E_{\mathrm{TC}}$ increases slightly with increasing small values of n (figure 10*a*), it is a strong function of cross-linking density. The inset in the figure shows that the yield strength increases monotonically with increasing cross-linking density and approaches a constant value. The nonlinear transition from small to large β is due to the nonlinear stress–strain behaviour of individual TC molecules. The curves reflect two failure mechanisms of

Downloaded from rsif.royalsocietypublishing.org on August 20, 2010

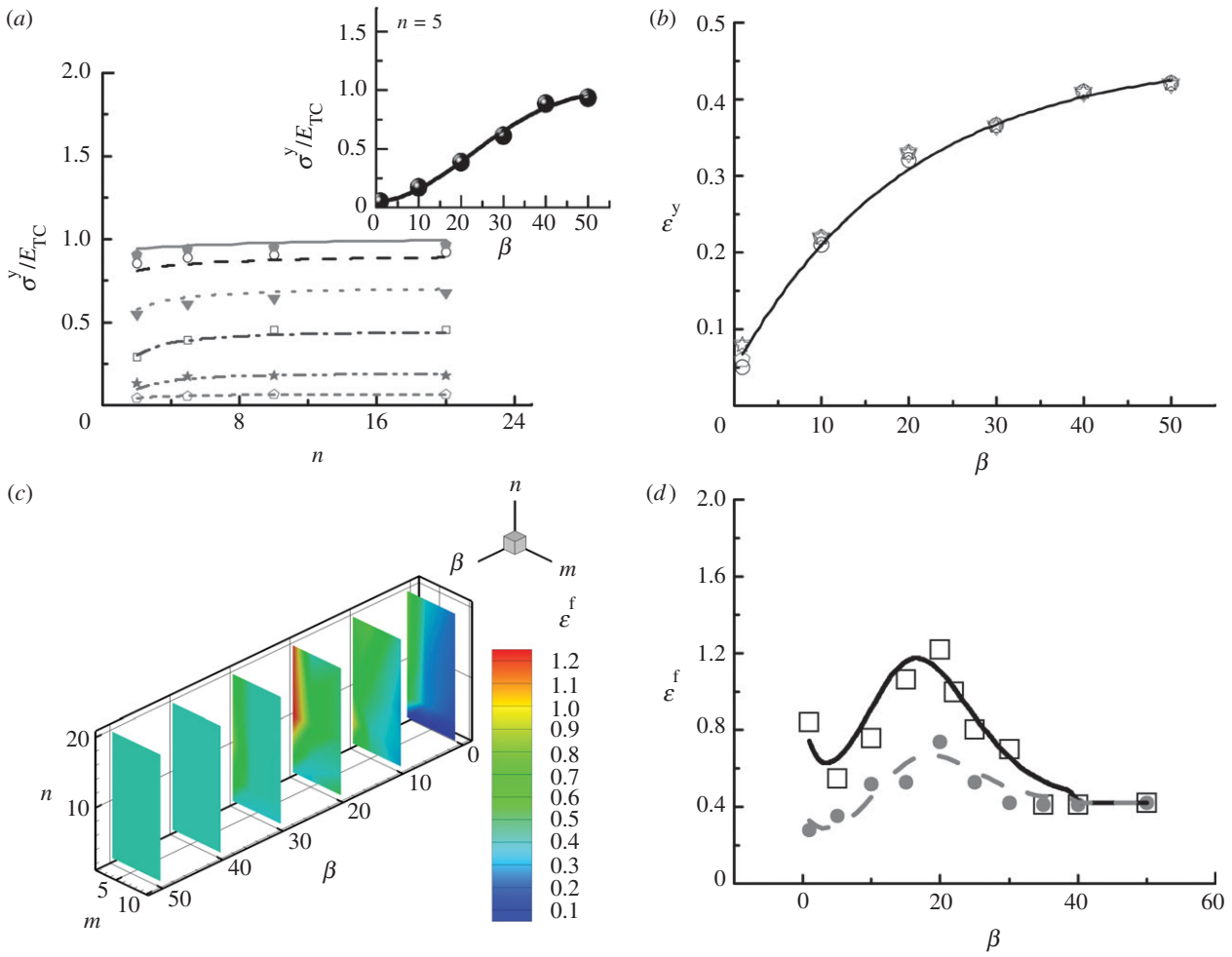

Figure 10. Results of MD and phenomenological model of collagen fibrils. (*a*) Yield strength σ^y/E_{TC} ($\beta = 1$: unfilled pentagon (MD), dashed grey line (phenomenological model); $\beta = 10$: star (MD), dotted dashed grey line (phenomenological model); $\beta = 20$: unfilled square (MD), dotted dashed black line (phenomenological model); $\beta = 30$: inverted triangle (MD), dotted grey line (phenomenological model); $\beta = 40$: open circle (MD), dashed black line (phenomenological model); $\beta = 50$: filled pentagon (MD), grey line (phenomenological model)); (*b*) yield strain ε^y (open circle, $n = 2$; pentagon, $n = 5$; inverted triangle, $n = 10$; star, $n = 20$; black line, phenomenological model); (*c*) fracture strain ε^f of MD simulations; (*d*) comparison of fracture strain ε^f of collagen fibrils with sample sizes ($n = 20$ and $m = 2$, black line (phenomenological model), unfilled square (MD); $n = 10$ and $m = 5$, dashed grey line (phenomenological model), grey circle (MD)). The parameters m and n are the number of TC molecules in length and width direction, and β is the cross-linking density factor.

collagen fibrils. For $\beta \sim 40$, the maximum adhesion forces transferred by the cross-links account for the maximum tensile strength of approximately 8.3 GPa of a single TC molecule (Buehler & Wong 2007). For $\beta < 40$, a graceful softening behaviour results from intermolecular shear (i.e. breaking cross-links and plastic slips of TC molecules). For $\beta \geq 40$, collagen fibrils fail in a brittle manner as a result of rupture of TC molecules.

Figure 10*b* shows the simulation results and the fitting curve for ε^y. Because the simulation results have a weak dependence on n, the data were fitted using the average over n at all values of cross-linking density. The nonlinearity of the curve is again due to the nonlinear mechanical responses of individual TC molecules. For $\beta \sim 40$, the dominant failure mechanism transitions from intermolecular shear to molecular fracture.

Cross-sections of the contour plot of ε^f calculated from the MD simulations, whose trends are more complex, are shown in figure 10*c*. A constant contour is observed for $\beta \geq 40$, since for those brittle fracture cases the fracture strain is equal to the yield strain. For $1 < \beta < 40$, ε^f is a function of m, n and β that increases with n and approaches ε^y for large m. As shown in figure 10*d*, the fracture strain–cross-linking density plot is bell shaped. The fitting equation describing these trends is

$$\varepsilon^f = \begin{cases} \varepsilon^y \left(1 - \dfrac{t_1}{m^{t_2}}\right) \\ \quad + \dfrac{t_3}{m^{t_2} b^{t_4}} \left(1 + t_5 \exp\left(-2 \ln \left(\dfrac{(\beta + t_6\beta^2) - t_7(1 + t_8\, m + t_9\, m^2)}{t_{10}(1 + t_{11} n + t_{12} n^2)} + t_{13} n\right)^2\right)\right) \\ \quad \times (1 + t_{14} \ln(n) + t_{15}(\ln(n))^2) \quad 1 < \beta < 40 \\ \varepsilon^y = q_1 + q_2 \exp\left(\dfrac{-\beta}{q_3}\right) \quad \beta \geq 40 \end{cases} \tag{3.11}$$

with the best-fit coefficients listed in table 1.

Downloaded from rsif.royalsocietypublishing.org on August 20, 2010

4. COMPARISON WITH EXPERIMENTAL RESULTS

Our computed small-strain and large-strain elastic moduli of collagen fibrils are approximately 5 and 35 GPa, respectively. The moduli slightly increase as the cross-linking density or the fibril width assumes larger values (figures 3 and 4). These computational results are close to a recent atomic force microscope nanoindentation experiment in air (Wenger *et al.* 2007), which found that the upper and lower limits of modulus were 5 and 11.5 GPa for collagen fibrils whose diameters ranged from 50 to 100 nm. However, this may be a coincidental agreement, since Wenger *et al.* computed the moduli by assuming the fibrils possess isotropic mechanical properties. The stiffness measured by applying tensile strain along the axial direction of type I collagen fibrils was smaller (Gupta *et al.* 2004; Shen *et al.* 2008).

The higher moduli in our simulations may result from an overestimation of mechanical stiffness properties at the molecular level, since the modulus of a single collagen molecule was found to form the upper limit of the modulus obtained from experiments (Buehler 2008). When considering the simplifications used to construct our molecular-level model (multiple repeats of 1QSU), it is not surprising to find that we arrived at a modulus that was too stiff. Ninety per cent of our model's amino acid triplets are Gly–Pro–Pro while only approximately 10 per cent of type I or type II collagen triplets have this sequence. This means that the helical stability of our model is probably much higher than that of the actual collagen molecule. The deeper minima of the model molecule's energy landscape would be expected to lead to a stiffer response of the model compared with the actual molecule. Recent MD simulations have shown that even small genetically based variations in the amino acid sequence can have a profound effect on the protein's biomechanical properties (Uzel & Buehler 2009). Furthermore, it is well known that when the prolines are hydroxylated, the secondary structure of each alpha chain forms a 7/2 helix while the unmodified prolines form a 10/3 helix (Brodsky & Persikov 2005). Real collagen molecules are thought to have stretches of both types of helices. The transition regions between these two helical forms may well be less tightly wound than the helices on either side. These would provide sections of the molecule with a lower stiffness than the flanking helices. Finally, it is thought that fibril-forming collagens have more than a dozen 'kink' regions where no helix is clearly defined (Shattuck 1994). These could also provide a softening mechanism for the overall molecule. The incorporation of more molecular-level details into the model might help to resolve the apparent discrepancies between experiment and simulation.

Other potential reasons for our stiffer modelled moduli include the presence of substantially higher deformation rates in simulation compared with experiment, which has been shown to lead to an overestimation of the molecular stiffness by a factor of approximately 1.75 (Gautieri *et al.* 2009*a*). Incorporating this effect, the modulus of collagen fibrils approaches a value around 2.9 GPa, closer to the tensile strain experimental results (Gupta *et al.* 2004; Shen *et al.* 2008). Furthermore, the computational setup considers perfectly two-dimensional staggered TC molecules, neglecting the influence from the more realistic three-dimensional woven configuration of collagen fibrils and the presence of molecular defects such as kinks and inclusions or free volume that exist in experimental specimens (Misof *et al.* 1997). Other reasons may include the difference in geometries and boundary conditions between simulation and experiments. For example, the maximum size of the specimens is 3 μm in length and 32 nm in width. While the gauge lengths of measured fibrils are of the same order of magnitude as our model, our maximum fibril width is substantially smaller than any of the experimentally tested fibrils (Gupta *et al.* 2004; Shen *et al.* 2008). Based on our results, this latter point is not expected to describe the theoretical/experimental discrepancy since we did not find any strong change in modulus with fibril width.

The yield strain of collagen fibrils is in the range 0.06–0.42 for different cross-link densities and sizes (figure 5), which is of the same order as corresponding experimental results (Shen *et al.* 2008). The yield strength predicted by the mesoscopic model is beyond 0.4 GPa, falling in the upper range of experimental findings (Shen *et al.* 2008). This suggests that mechanisms for yield which are at play in the experimental system have not been captured by our model. In our simulation, the yield strength increases when cross-linking density or width of the collagen fibril increases. However, experimental studies (Shen *et al.* 2008) showed that the yield strain decreases for specimens with larger volume. The experimental observations and the simulation results are not necessarily contradictory since our model ignored the existence of initial defects, which usually increases with volume in real specimens. In addition, the cross-linking density is uniform in the current model, while it could be a distributed function in experimentally tested specimens.

Owing to the complexity of the cross-linking densities and existing defects of real specimens, it is difficult to verify the trends of fracture strains presented in this study using available experimental results. We expect that new experiments will be stimulated to confirm the findings put forth based on the multi-scale simulations reported here. On the other hand, to simulate the mechanical responses of real collagen fibrils, the numerical model needs to be further improved to capture the distribution of cross-linking density and defects and to consider the varying amino acid sequence along the molecular axis. Current efforts are under way to incorporate these effects in molecular modelling (Uzel & Buehler 2009).

5. CONCLUSION

We applied a mesoscopic reactive molecular model to study the responses of collagen fibrils upon uniaxial tension, focusing specifically on the effect of fibril width and length on the mechanical behaviour. Dependence of post-peak behaviour of the stress–strain curve of a finite size relatively short fibril on cross-linking density is consistent with the results obtained previously using

Downloaded from rsif.royalsocietypublishing.org on August 20, 2010

periodic boundary conditions across the width. This study showed, however, that the post-peak stress behaviour is highly dependent on fibril length, width and cross-linking density. These size effects appear to reach asymptotic values in the range of a few tens of molecules in the length and width directions. All fibril-forming collagens produce fibrils that are much longer than this. In addition, most normal type I collagen fibrils are much wider than this. Thus, we would not expect to see length dependence effects in tissue fibrils that possess no defects. However, if the defect distribution in tissue fibrils presents in such a way that the fibrils display stress concentrations over lengths of a few micrometres or less, then the size dependence effects we show are expected to be seen in experimental data. Moreover, non-type I collagen fibrils with diameters of a few tens of molecules are often present in tissues (e.g. type XI/II heterofibrils in cartilage). Thus, if it is possible to experimentally measure such thin fibril samples, we would expect strong size effects to govern the mechanical response of collagen fibrils in these tissues. Visualization of the deformation of the finite size collagen fibrils up to fracture, presented here for the first time by using the slip vector approach, demonstrated that the underlying micromechanisms could be explained by extension of and relative sliding between TC molecules. The results were used to construct a simple analytical model and curve-fitting expressions for yield stress, yield strain and fracture strain. Our phenomenological model is expected to be of use to researchers who do not have the resources to implement the full hierarchical model used to fit the functions described in the phenomenological model.

Our study illustrates the use of a multi-scale approach, in which a hierarchy of simulation techniques is used to derive the macroscale constitutive behaviour of collagen fibrils. Future work could also include a study of the effect of structural defects, sequence variations and a more detailed modelling of intermolecular cross-links. Applications of this hierarchical approach could be found in the study of genetic diseases or tissue injuries, where deformation mechanisms and associated mechanical properties are crucial to understand physiologically relevant materials phenomena (Gautieri *et al.* 2009*b*).

R.B. and S.J.E. acknowledge support from the National Science Foundation (grant no. 0532320) and the National Institutes of Health (grant no. 1 R21 EB004985-01A1). M.J.B. acknowledges support through a National Science Foundation CAREER award (CMMI-0642545) and the Army Research Office (W911NF-06-1-0291). Y.T. and R.B. also acknowledge support from the James L. Record Chair and the computing resources provided by the Minnesota Supercomputer Institute (MSI).

REFERENCES

Abrahams, M. 1967 Mechanical behaviour of tendon *in vitro*. A preliminary report. *Med. Biol. Eng.* **5**, 433–443. (doi:10.1007/BF02479137)

Akizuki, S., Mow, V. C., Muller, F., Pita, J. C., Howell, D. S. & Manicourt, D. H. 1986 Tensile properties of human knee-joint cartilage. 1. Influence of ionic conditions, weight bearing, and fibrillation on the tensile modulus. *J. Orthop. Res.* **4**, 379–392. (doi:10.1002/jor.1100040401)

Alberts, B., Johnson, A., Lewis, J., Raff, M., Roberts, K. & Walter, P. 2002 *Molecular biology of the cell*. New York, NY: Garland Science, Taylor & Francis.

Bailey, A. J. 2001 Molecular mechanisms of ageing in connective tissues. *Mech. Ageing Dev.* **122**, 735–755. (doi:10.1016/S0047-6374(01)00225-1)

Bella, J., Eaton, M., Brodsky, B. & Berman, H. M. 1994 Crystal-structure and molecular-structure of a collagen-like peptide at 1.9-angstrom resolution. *Science* **266**, 75–81. (doi:10.1126/science.7695699)

Bigliani, L. U., Pollock, R. G., Soslowsky, L. J., Flatow, E. L., Pawluk, R. J. & Mow, V. C. 1992 Tensile properties of the inferior glenohumeral ligament. *J. Orthop. Res.* **10**, 187–197. (doi:10.1002/jor.1100100205)

Bonar, L. C., Lees, S. & Mook, H. A. 1985 Neutron-diffraction studies of collagen in fully mineralized bone. *J. Mol. Biol.* **181**, 265–270. (doi:10.1016/0022-2836(85)90090-7)

Bozec, L. & Horton, M. 2005 Topography and mechanical properties of single molecules of type I collagen using atomic force microscopy. *Biophys. J.* **88**, 4223–4231. (doi:10.1529/biophysj.104.055228)

Bozec, L., van der Heijden, G. & Horton, M. 2007 Collagen fibrils: nanoscale ropes. *Biophys. J.* **92**, 70–75. (doi:10.1529/biophysj.106.085704)

Brodsky, B. & Persikov, A. V. 2005 Molecular structure of the collagen triple helix. In *Fibrous proteins: coiled-coils, collagen and elastomers* (eds D. A. D. Parry & J. M. Squire). Advances in Protein Chemistry, vol. 70, pp. 301–339. San Diego, CA: Elsevier Academic Press.

Buehler, M. J. 2006*a* Atomistic and continuum modeling of mechanical properties of collagen: elasticity, fracture, and self-assembly. *J. Mater. Res.* **21**, 1947–1961. (doi:10.1557/jmr.2006.0236)

Buehler, M. J. 2006*b* Nature designs tough collagen: explaining the nanostructure of collagen fibrils. *Proc. Natl Acad. Sci. USA* **103**, 12 285–12 290. (doi:10.1073/pnas.0603216103)

Buehler, M. J. 2008 Nanomechanics of collagen fibrils under varying cross-link densities: atomistic and continuum studies. *J. Mech. Behav. Biomed. Mater.* **1**, 59–67. (doi:10.1016/j.jmbbm.2007.04.001)

Buehler, M. J. & Wong, S. Y. 2007 Entropic elasticity controls nanomechanics of single tropocollagen molecules. *Biophys. J.* **93**, 37–43. (doi:10.1529/biophysj.106.102616)

Catanese, J., Iverson, E. P., Ng, R. K. & Keaveny, T. M. 1999 Heterogeneity of the mechanical properties of demineralized bone. *J. Biomech.* **32**, 1365–1369. (doi:10.1016/S0021-9290(99)00128-1)

Christiansen, D. L., Huang, E. K. & Silver, F. H. 2000 Assembly of type I collagen: fusion of fibril subunits and the influence of fibril diameter on mechanical properties. *Matrix Biol.* **19**, 409–420. (doi:10.1016/S0945-053X(00)00089-5)

Diamant, J., Arridge, R. G. C., Baer, E., Litt, M. & Keller, A. 1972 Collagen—ultrastructure and its relation to mechanical properties as a function of aging. *Proc. R. Soc. Lond. B* **180**, 293–315. (doi:10.1098/rspb.1972.0019)

Folkhard, W., Geercken, W., Knorzer, E., Mosler, E., Nemetschek-Gansler, H., Nemetschek, T. & Koch, M. H. J. 1987 Structural dynamic of native tendon collagen. *J. Mol. Biol.* **193**, 405–407. (doi:10.1016/0022-2836(87)90228-2)

Fratzl, P., Misof, K., Zizak, I., Rapp, G., Amenitsch, H. & Bernstorff, S. 1998 Fibrillar structure and mechanical properties of collagen. *J. Struct. Biol.* **122**, 119–122. (doi:10.1006/jsbi.1998.3966)

Downloaded from rsif.royalsocietypublishing.org on August 20, 2010

Freed, A. D. & Doehring, T. C. 2005 Elastic model for crimped collagen fibrils. *J. Biomech. Eng.* **127**, 587–593. (doi:10.1115/1.1934145)

Fritsch, A. & Hellmich, C. 2007 'Universal' microstructural patterns in cortical and trabecular, extracellular and extravascular bone materials: micromechanics-based prediction of anisotropic elasticity. *J. Theor. Biol.* **244**, 597–620. (doi:10.1016/j.jtbi.2006.09.013)

Fritsch, A., Hellmich, C. & Dormieux, L. 2009 Ductile sliding between mineral crystals followed by rupture of collagen crosslinks: experimentally supported micromechanical explanation of bone strength. *J. Theor. Biol.* **260**, 230–252. (doi:10.1016/j.jtbi.2009.05.021)

Gautieri, A., Buehler, M. J. & Redaelli, A. 2009*a* Deformation rate controls elasticity and unfolding pathway of single tropocollagen molecules. *J. Mech. Behav. Biomed. Mater.* **2**, 130–137. (doi:10.1016/j.jmbbm.2008.03.001)

Gautieri, A., Uzel, S., Vesentini, S., Redaelli, A. & Buehler, M. J. 2009*b* Molecular and mesoscale mechanisms of osteogenesis imperfecta disease in collagen fibrils. *Biophys. J.* **97**, 857–865. (doi:10.1016/j.bpj.2009.04.059)

Gentleman, E., Lay, A. N., Dickerson, D. A., Nauman, E. A., Livesay, G. A. & Dee, K. C. 2003 Mechanical characterization of collagen fibers and scaffolds for tissue engineering. *Biomaterials* **24**, 3805–3813. (doi:10.1016/S0142-9612(03)00206-0)

Gupta, H. S., Messmer, P., Roschger, P., Bernstorff, S., Klaushofer, K. & Fratzl, P. 2004 Synchrotron diffraction study of deformation mechanisms in mineralized tendon. *Phys. Rev. Lett.* **93**, 158101. (doi:10.1103/PhysRevLett.93.158101)

Gutsmann, T., Fantner, G. E., Venturoni, M., Ekani-Nkodo, A., Thompson, J. B., Kindt, J. H., Morse, D. E., Fygenson, D. K. & Hansma, P. K. 2003 Evidence that collagen fibrils in tendons are inhomogeneously structured in a tubelike manner. *Biophys. J.* **84**, 2593–2598. (doi:10.1016/S0006-3495(03)75064-4)

Gutsmann, T., Fantner, G. E., Kindt, J. H., Venturoni, M., Danielsen, S. & Hansma, P. K. 2004 Force spectroscopy of collagen fibers to investigate their mechanical properties and structural organization. *Biophys. J.* **86**, 3186–3193. (doi:10.1016/S0006-3495(04)74366-0)

Hellmich, C., Barthelemy, J. F. & Dormieux, L. 2004 Mineral-collagen interactions in elasticity of bone ultrastructure—a continuum micromechanics approach. *Eur. J. Mech. A Solids* **23**, 783–810. (doi:10.1016/j.euromechsol.2004.05.004)

Hodge, A. J. & Petruska, J. A. 1963 In *Recent studies with the electron microscope on ordered aggregates of the tropocollagen molecule* (ed. G. N. Ramachandran), pp. 289–300. New York, NY: Academic Press.

Israelowitz, M., Rizvi, S. W. H., Kramer, J. & von Schroeder, H. P. 2005 Computational modeling of type I collagen fibers to determine the extracellular matrix structure of connective tissues. *Protein Eng. Des. Sel.* **18**, 329–335. (doi:10.1093/protein/gzi037)

Jager, I. & Fratzl, P. 2000 Mineralized collagen fibrils: a mechanical model with a staggered arrangement of mineral particles. *Biophys. J.* **79**, 1737–1746. (doi:10.1016/S0006-3495(00)76426-5)

Jirasek, M. & Bazant, Z. P. 2001 *Inelastic analysis of structures*. Chichester, UK: John Wiley & Sons, Ltd.

Kadler, K. E., Holmes, D. F., Trotter, J. A. & Chapman, J. A. 1996 Collagen fibril formation. *Biochem. J.* **316**, 1–11.

Kramer, R. Z., Venugopal, M. G., Bella, J., Mayville, P., Brodsky, B. & Berman, H. M. 2000 Staggered molecular packing in crystals of a collagen-like peptide with a single charged pair. *J. Mol. Biol.* **301**, 1191–1205. (doi:10.1006/jmbi.2000.4017)

Lees, S. 1986 Water content in type I collagen tissues calculated from the generalized packing model. *Int. J. Biol. Macromol.* **8**, 66–72. (doi:10.1016/0141-8130(86)90001-2)

Lees, S. 1987 Considerations regarding the structure of the mammalian mineralized osteoid from viewpoint of the generalized packing model. *Connect. Tissue Res.* **16**, 281–303. (doi:10.3109/03008208709005616)

Lees, S., Pineri, M. & Escoubes, M. 1984*a* A generalized packing model for type I collagen. *Int. J. Biol. Macromol.* **6**, 133–136. (doi:10.1016/0141-8130(84)90053-9)

Lees, S., Bonar, L. C. & Mook, H. A. 1984*b* A study of dense mineralized tissue by neutron-diffraction. *Int. J. Biol. Macromol.* **6**, 321–326. (doi:10.1016/0141-8130(84)90017-5)

Li, L. P., Buschmann, M. D. & Shirazi-Adl, A. 2000 A fibril reinforced nonhomogeneous poroelastic model for articular cartilage: inhomogeneous response in unconfined compression. *J. Biomech.* **33**, 1533–1541. (doi:10.1016/S0021-9290(00)00153-6)

Lodish, H., Berk, A., Zipursky, S. L., Matsudaria, P., Baltimore, D. & Darnell, J. E. 1999 *Molecular cell biology*. New York, NY: W H Freeman & Co.

Lorenzo, A. C. & Caffarena, E. R. 2005 Elastic properties, Young's modulus determination and structural stability of the tropocollagen molecule: a computational study by steered molecular dynamics. *J. Biomech.* **38**, 1527–1533. (doi:10.1016/j.jbiomech.2004.07.011)

Misof, K., Rapp, G. & Fratzl, P. 1997 A new molecular model for collagen elasticity based on synchrotron x-ray scattering evidence. *Biophys. J.* **72**, 1376–1381. (doi:10.1016/S0006-3495(97)78783-6)

Mooney, S. D., Huang, C. C., Kollman, P. A. & Klein, T. E. 2001 Computed free energy differences between point mutations in a collagen-like peptide. *Biopolymers* **58**, 347–353. (doi:10.1002/1097-0282(200103)58:3<347::AID-BIP1011>3.0.CO;2-M)

Mooney, S. D., Kollman, P. A. & Klein, T. E. 2002 Conformational preferences of substituted prolines in the collagen triple helix. *Biopolymers* **64**, 63–71. (doi:10.1002/bip.10123)

Nikolov, S. & Raabe, D. 2008 Hierarchical modeling of the elastic properties of bone at submicron scales: the role of extrafibrillar mineralization. *Biophys. J.* **94**, 4220–4232. (doi:10.1529/biophysj.107.125567)

Orgel, J., Irving, T. C., Miller, A. & Wess, T. J. 2006 Microfibrillar structure of type I collagen *in situ*. *Proc. Natl Acad. Sci. USA* **103**, 9001–9005. (doi:10.1073/pnas.0502718103)

Ottani, V., Martini, D., Franchi, M., Ruggeri, A. & Raspanti, M. 2002 Hierarchical structures in fibrillar collagens. *Micron* **33**, 587–596. (doi:10.1016/S0968-4328(02)00033-1)

Parry, D. A. D. 1988 The molecular and fibrillar structure of collagen and its relationship to the mechanical properties of connective tissue. *Biophys. Chem.* **29**, 195–209. (doi:10.1016/0301-4622(88)87039-X)

Plimpton, S. 1995 Fast parallel algorithms for short-range molecular-dynamics. *J. Comput. Phys.* **117**, 1–19. (doi:10.1006/jcph.1995.1039)

Purslow, P. P., Wess, T. J. & Hukins, D. W. L. 1998 Collagen orientation and molecular spacing during creep and stress-relaxation in soft connective tissues. *J. Exp. Biol.* **201**, 135–142.

Rice, R. V., Maser, M. D., Casassa, E. F. & Kerwin, R. E. 1964 On length + molecular weight of tropocollagen from calf skin. *Arch. Biochem. Biophys.* **105**, 409–423. (doi:10.1016/0003-9861(64)90025-6)

Downloaded from rsif.royalsocietypublishing.org on August 20, 2010

Schmitt, F. O., Hall, C. E. & Jakus, M. A. 1942 Electron microscope investigations of the structure of collagen. *J. Cell. Comp. Physiol.* **20**, 11–33. (doi:10.1002/jcp.1030200103)

Shattuck, M. B. 1994 *Scanning force microscopy of collagen and biological materials at low temperature, in bioengineering*. San Francisco, CA: University of California at Berkeley.

Shen, Z. L., Dodge, M. R., Kahn, H., Ballarini, R. & Eppell, S. J. 2008 Stress-strain experiments on individual collagen fibrils. *Biophys. J.* **95**, 3956–3963. (doi:10.1529/biophysj.107.124602)

Soulhat, J., Buschmann, M. D. & Shirazi-Adl, A. 1999 A fibril-network-reinforced biphasic model of cartilage in unconfined compression. *J. Biomech. Eng.* **121**, 340–347. (doi:10.1115/1.2798330)

Sun, Y. L., Luo, Z. P., Fertala, A. & An, K. N. 2002 Direct quantification of the flexibility of type I collagen monomer. *Biochem. Biophys. Res. Commun.* **295**, 382–386. (doi:10.1016/S0006-291X(02)00685-X)

Sun, Y. L., Luo, Z. P., Fertala, A. & An, K. N. 2004 Stretching type II collagen with optical tweezers. *J. Biomech.* **37**, 1665–1669. (doi:10.1016/j.jbiomech.2004.02.028)

Tang, H., Buehler, M. J. & Moran, B. 2009 A constitutive model of soft tissue: from nanoscale collagen to tissue continuum. *Ann. Biomed. Eng.* **37**, 1117–1130. (doi:10.1007/s10439-009-9679-0)

Uzel, S. & Buehler, M. J. 2009 Nanomechanical sequencing of collagen: tropocollagen features heterogeneous elastic properties at the nanoscale. *Integr. Biol.* **1**, 452–459. (doi:10.1039/b906864c)

Veld, P. J. & Stevens, M. J. 2008 Simulation of the mechanical strength of a single collagen molecule. *Biophys. J.* **95**, 33–39. (doi:10.1529/biophysj.107.120659)

Wenger, M. P. E., Bozec, L., Horton, M. A. & Mesquida, P. 2007 Mechanical properties of collagen fibrils. *Biophys. J.* **93**, 1255–1263. (doi:10.1529/biophysj.106.103192)

Wilson, W., van Donkelaar, C. C., van Rietbergen, B., Ito, K. & Huiskes, R. 2004 Stresses in the local collagen network of articular cartilage: a poroviscoelastic fibril-reinforced finite element study. *J. Biomech.* **37**, 357–366. (doi:10.1016/S0021-9290(03)00267-7)

Wilson, W., van Donkelaar, C. C., van Rietbergen, B. & Huiskes, R. 2005 A fibril-reinforced poroviscoelastic swelling model for articular cartilage. *J. Biomech.* **38**, 1195–1204. (doi:10.1016/j.jbiomech.2004.07.003)

Zimmerman, J. A., Kelchner, C. L., Klein, P. A., Hamilton, J. C. & Foiles, S. M. 2001 Surface step effects on nanoindentation. *Phys. Rev. Lett.* **87**, 165507. (doi:10.1103/PhysRevLett.87.165507)